AFRL-AFOSR-JP-TR-2016-0097

High density metamaterials for visible light

Dao Hua Zhang
NANYANG TECHNOLOGICAL UNIVERSITY

11/28/2016
Final Report

Air Force Research Laboratory
AF Office Of Scientific Research (AFOSR)/ IOA
Arlington, Virginia 22203
Air Force Materiel Command

REPORT DOCUMENTATION PAGE

Form Approved
OMB No. 0704-0188

1. REPORT DATE *(DD-MM-YYYY)*	2. REPORT TYPE	3. DATES COVERED *(From - To)*
05-12-2016	Final	16 Jul 2014 to 15 Jul 2016

4. TITLE AND SUBTITLE
High density metamaterials for visible light

5a. CONTRACT NUMBER

5b. GRANT NUMBER
FA2386-14-1-0013

5c. PROGRAM ELEMENT NUMBER
61102F

6. AUTHOR(S)
Dao Hua Zhang

5d. PROJECT NUMBER

5e. TASK NUMBER

5f. WORK UNIT NUMBER

7. PERFORMING ORGANIZATION NAME(S) AND ADDRESS(ES)
NANYANG TECHNOLOGICAL UNIVERSITY
50 NANYANG AVENUE
SINGAPORE, 639798 SG

8. PERFORMING ORGANIZATION REPORT NUMBER

9. SPONSORING/MONITORING AGENCY NAME(S) AND ADDRESS(ES)
AOARD
UNIT 45002
APO AP 96338-5002

10. SPONSOR/MONITOR'S ACRONYM(S)
AFRL/AFOSR IOA

11. SPONSOR/MONITOR'S REPORT NUMBER(S)
AFRL-AFOSR-JP-TR-2016-0097

12. DISTRIBUTION/AVAILABILITY STATEMENT
A DISTRIBUTION UNLIMITED: PB Public Release

13. SUPPLEMENTARY NOTES

14. ABSTRACT
Investigate a large exposure dose and characterize sub-100-nm sized split-ring resonator metamaterial structures in visible range which are potentially useful for cloaking and ultrasensitive biochemical sensors, and to explore the limit of resonator size with gold first and then extend the techniques to other metals for better characteristics. Bio-chemical sensors will be developed based on different split ring resonator geometries. In addition, metamaterials on flexible substrates for cloaking application for visible light will also be explored in this proposed effort.

15. SUBJECT TERMS
Multimodality, Network Congestion, Network Vulnerability

16. SECURITY CLASSIFICATION OF:			17. LIMITATION OF ABSTRACT	18. NUMBER OF PAGES	19a. NAME OF RESPONSIBLE PERSON
a. REPORT	b. ABSTRACT	c. THIS PAGE			HONG, SENG
Unclassified	Unclassified	Unclassified	SAR	18	19b. TELEPHONE NUMBER *(Include area code)* 315-229-3519

Final Report for AOARD Grant FA2386-14-1-0013

High density metamaterials for visible light

Date Nov. 11th, 2016

Key Researchers involved in the proposed project and address:
Prof. Dao-Hua ZHANG ((Principal Investigator), Nanyang Technological University (NTU), 50 Nanyang Avenue 639798, Singapore
Tel: 65-67904841; Email: edhzhang@ntu.edu.sg
Prof. Qihua XIONG, (NTU), 50 Nanyang Avenue 639798, Singapore
Dr. Landobasa Y. M. Tobing, (NTU), 50 Nanyang Avenue 639798, Singapore
Professor A. G. U. Perera, Georgia State University, USA

Period of Performance: 16 Jul 2014 to 15 Jul 2016

Abstract
In this project, we aimed to design, fabricate and characterize sub-100-nm sized split-ring resonator metamaterial structures in visible range which are potentially useful for cloaking and ultrasensitive biochemical sensors. We explore the limit of resonator size and also develop the application of SRR metamaterials for Bio-chemical sensing. Using our sonicated cold development electron beam lithography process that has recently been shown to overcome the tradeoff between resolution and throughput, we designed, fabricated, and characterized ultrasmall split-ring resonator metamaterial structures covering from ultraviolet to near-infrared frequency range. The smallest achievable dimensions were explored, enabling various investigations ranging from the interaction of resonance modes with the interband transition of a metal, to kinetic inductance limitation for the achievable magnetic resonance in split ring resonators. Rotationally symmetric resonator geometries were studied in detail and characterized in terms of their capability as a robust and efficient sensing platform.

1. Introduction
Metamaterial is formed out of an array of deep subwavelength metallic nanostructures that are designed to produce novel optical properties. The most widely studied aspect in metamaterials is the ability for light confinement in ultrasmall dimensions, which serves as the platform for light-matter interaction at the nanoscale [1]–[4], designing optical nanoantenna [5]–[7], and for biochemical sensing [8]–[16]. However, as the dimensional requirements are proportional to its operational wavelength, the metamaterial fabrication becomes increasingly challenging towards

visible spectrum operation. This is attributable to the inherent tradeoff between resolution and throughput in any lithography process, where smaller dimensions can be patterned at the expense of large exposure dose, making large-scale fabrication of ultrasmall resonators not practical. Many methods have been proposed to overcome this challenge, including the use of self-assembly process in nanosphere lithography (NSL) [17], [18], and the combination of laser-induced-transfer (LIT) and focused-ion-beam (FIB) [19]. However, these methods lack the lithographic flexibility inherent in electron-beam-lithography (EBL) process and often involve complex fabrication steps. Therefore, the standard EBL method is still preferable over these non-standard methods.

We have proposed an EBL process that addresses the inherent tradeoff between resolution and throughput, where a mild sonication is introduced at specific timing for a specific duration during a cold development [20]–[22]. Based on this process, gold (Au) and silver (Ag) split-ring resonators (SRR) have been demonstrated, with the resonator size as small as ~60 nm and observed magnetic frequencies in the mid-visible spectrum range [13], [23]. Recently, we further improve this nanofabrication capability for realizing even smaller resonators, and show that such ultrasmall dimensions makes possible the experimental investigation of self-limiting mechanism for the achievable magnetic resonance that was theoretically studied over a decade ago [24]–[26]. We demonstrate aluminium split-ring resonators working on ultraviolet frequency spectrum, and discuss its unique optical properties and fabrication challenges [27]. Finally, we investigate variety of rotationally symmetric structures aimed for biosensing applications.

2. Experiment, Results, and Discussion

(1) Observation of the kinetic inductance limitation for the fundamental magnetic resonance in ultrasmall gold v-shape split ring resonators [Adv. Opt. Mater. 4, 1047 (2016)]

The kinetic inductance limitation has been proposed as the fundamental limitation for the attainable magnetic resonance frequency in SRRs, but its experimental verification remains challenging owing to the stringent dimensional requirements in the resonator nanofabrication. In this work, we report the first experimental observation for such saturation effects with saturated frequency at 520 THz using gold *v*-shape split ring resonators. The interplay between electric dipole and magnetic dipole as a function of SRR opening angle is theoretically studied and experimentally observed, showing the dramatic increase of intensity buildup and resonance contrast as the dominant mode changes from electric to magnetic.

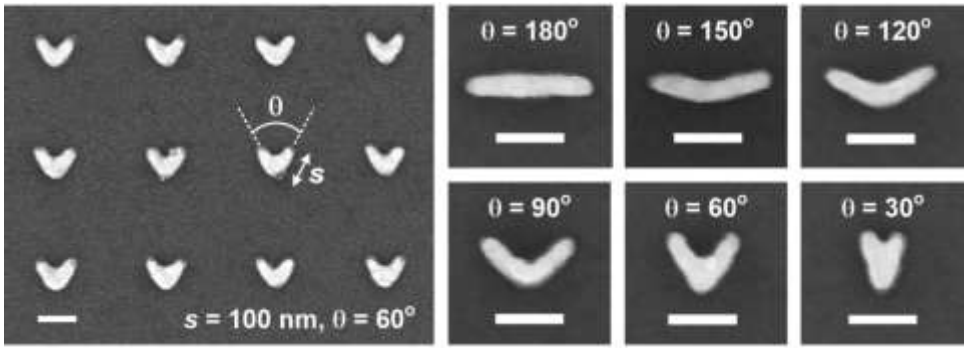

Figure 1. The *v*-SRRs in square lattice configuration. The fabricated SRRs are of 30 nm metal thickness and 25-nm metal width. The opening angles were varied from $\theta = 180^o$ (horizontal nanorod) to $\theta = 0^o$ (vertical nanorod). The scale bars correspond to 100 nm.

The *v*-SRRs were fabricated by the sonicated cold development process with achievable pitch of ~40 nm. [20], [22] After lithographic patterning, the samples were evaporated with 2-nm thick titanium adhesion layer and 30-nm thick gold on ITO-coated glass, followed by lift-off in *n*-methyl pyrrolidone (NMP) for 10 minutes. Figure 1 shows the examples of the fabricated *v*-SRRs, which are characterized by the arm length (*s*) and the opening angle (θ). The left panel shows the *v*-SRRs with 100-nm arm length and 60^o opening angle; while the right panels show the *v*-SRRs with opening angles varied from $\theta = 180^o$ to $\theta = 30^o$, for a fixed arm length of 100 nm. Figure 2 shows FDTD calculations of the intensity buildup in the *v*-SRR as a function of the opening angle, with its corresponding electromagnetic fields distribution. The typical side and top view of the E_x-field distribution at the fundamental magnetic resonances is shown in the insets of Figure 2a, while the intensity buildup is numerically measured at the point "B" in the simulations. The intensity buildup is rather flat at large angles, but begins to increase sharply below $\theta \sim 50^o$. This remains true as the arm length is varied from $s = 100$ nm to $s = 60$ nm. The electromagnetic field distributions of *v*-SRR are presented in Figure 2b, showing the evolution from electric-dipole to magnetic-dipole as the opening angle is decreased from $\theta = 180^o$ to $\theta = 30^o$. At $\theta = 180^o$, we have a nanorod situation where the E_x-fields are confined at both tips, with E_y-fields and H_z-fields symmetric with respect to the horizontal axis.

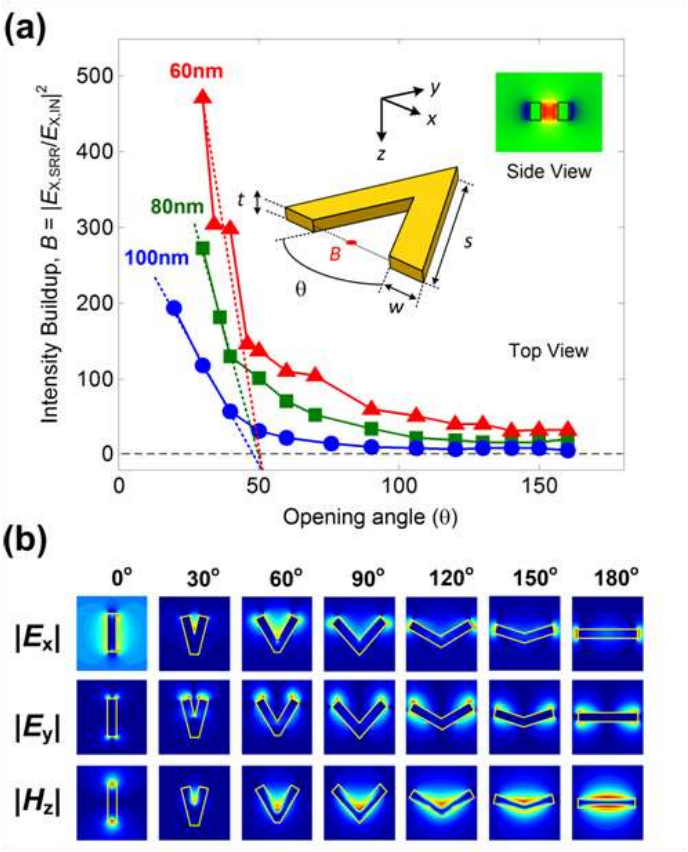

Figure 2. Mode evolution from electric dipole-like to magnetic dipole in *v*-SRR. (a) Intensity buildup as a function of opening angle. (b) The evolution of electromagnetic field distributions ($|E_x|$,$|E_y|$,$|H_z|$) of *v*-SRR along with increasing opening angles.

In this case, the resonator behaves as a plasmonic particle, with pure electric dipole resonances corresponding to plasmonic oscillation in the direction of incidence polarization. As the angle is decreased, the accumulated electric charges (from the two tips) begin to interact capacitively, skewing the E_y-field and H_z-field distributions towards the inner side of the *v*-SRR. Thus, both electric-dipole and magnetic-dipole are generated in this situation, where the former is due to the conduction current from plasmonic oscillation in the longitudinal direction, and the latter is due to displacement current from the capacitive interaction between the *v*-SR R tips. As the gap separation decreases, the ohmic resistance remains unchanged due to a fixed metal length, while the capacitive impedance becomes smaller. This leads to a higher conduction current and stronger E_x-fields in the SRR gap. Thus, the electric field enhancement in the SRR gaps translates to the magnetic dipole strength, suggesting that the excitation of magnetic-dipole is more preferable at small opening angles. This is indeed depicted by the mode evolution in Figure 2b, where the transition from plasmonic particle (corresponding to electric dipole) to split-ring resonator (corresponding to magnetic dipole) occurs at $\theta \sim 50^o$. The lateral sizes of the *v*-SRR in the X and Y direction for a given opening angle (θ) and arm length (s) are given by $s_X(\theta) = 2s\sin(\theta/2)$ and $s_Y(\theta) = s\cos(\theta/2)$, respectively. Thus, the condition where the resonator sizes are the same in both direction, i.e., $s_X(\theta) = s_Y(\theta)$, is satisfied at $\theta_T = 2\tan^{-1}(1/2) \cong 53°$, which is interestingly close to the transition angle observed in Figure 2a. Thus, from plasmonic particle perspective, the resonance for X-polarization is longer (shorter) than that for Y-polarization at $\theta > \theta_T$ ($\theta < \theta_T$). As the resonance wavelength of m_0 is always longer than that of e_0 [x], it then follows that the m_0 resonance behaves more as an electric dipole at $\theta > \theta_T$ and more as a magnetic dipole at $\theta < \theta_T$. This could be the likely cause for the transition from electric-dipole to magnetic-dipole at $\theta \sim 50^o$ in Figure 2a.

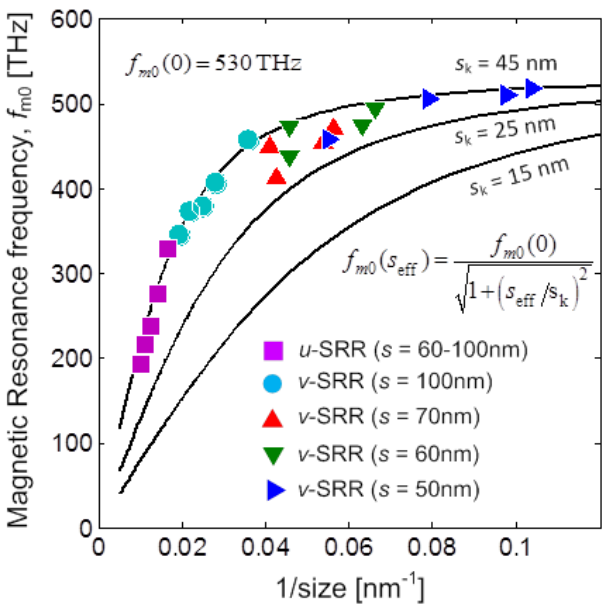

Figure 3. Saturation of the fundamental magnetic resonances in split ring resonator. The fittings based on s_K = 15 nm, s_K = 25 nm, and s_K = 45 nm for a fixed saturation frequency of $f_{m0}(0)$ = 530 THz are denoted in solid lines. For all the *u*-SRRs and *v*-SRRs, the feature width and thickness is 25 nm and 30 nm, respectively. At increasing "1/size" order, there are 5 variations for *v*-SRR with *s* = 100 nm, and 4 variations for *v*-SRRs with *s* = 50-70 nm. The variations for *s* = 100 nm are (1) θ = 90°, (2) θ = 60°, (3) θ = 30°, *d* = 12 nm, (4) θ = 30°, *d* = 8 nm, (5) θ = 30°, *d* = 0 nm, while the variations for *s* = 50-70 nm are (1) θ = 90°, (2) θ = 60°, (3) θ = 30°, *d* = 14 nm, (4) θ = 30°, *d* = 12 nm.

In order to demonstrate the magnetic resonance frequency saturation resulting from kinetic inductance limitation, we show in Figure 3 the mapping of m_0 mode as a function of inverse resonator size. Here, the resonance positions of the *v*-SRRs are combined with those of the *u*-SRRs from our previous work. [13] There are 5 geometric variations for *v*-SRRs with s = 100 nm, while there are 4 geometric variations for v-SRR with *s* = 50-70 nm. The resonator size (s_{eff}) of *v*-SRRs is approximated as $s_{eff} \cong (A_{SRR})^{1/2}$, where $A_{SRR} = 1/2 \times (base) \times (height)$ is the area of the *v*-SRR with base and height obtained from SEM inspections. The resonator size for the *u*-SRR structures is defined as the length of the bottom arm. The saturation effect can be seen clearly at a very small resonator size, where the m_0 mode saturates at ~520 THz (578 nm). The same saturation effect is observed for the e_0 mode (not shown here), where the e_0 mode saturates at ~530 THz (565 nm). Note that the observed two saturation frequencies are still lower than the interband transition of gold at 556 THz (539 nm). This is as expected since the plasmonic oscillation is significantly suppressed by the interband transition. The role of interband transition in the magnetic resonance is also investigated numerically, where finite difference time domain calculations are performed based on Drude metals and on gold permittivity according to Johnson and Christy [28].

(2) Preferential excitation of the hybrid magnetic-electric mode as a limiting mechanism for achievable fundamental magnetic resonance in planar aluminium nanostructures [Adv. Mater. 28, 889 (2015)]

Owing to its bulk plasma oscillation in the deep ultraviolet and higher free electron density, aluminum nanostructures has been shown to exhibit better plasmonic performance as compared

to its gold and silver counterparts in the UV-Vis frequency range [29], [30]. Different kinds of aluminum nanostructures have been explored [31]–[34], and their electric dipole modes have been experimentally studied and mapped [31]. Meanwhile, the magnetic dipole resonances have also been demonstrated at up to 532nm in planar split ring resonator (SRR) structure [35], which also proved useful for enhancing Raman signal in the grapheme [15]. Interestingly, the realization of magnetic resonances in the deep visible spectrum remains challenging despite the fact that the fundamental kinetic inductance limitation has not yet occurred in such frequency range. This is mainly attributed to the aluminum interband transition (at 800 nm) that is known to impart red shifts of the resonance modes. Thus, the existing size dependence of split ring resonators [36], coupled with the need for compensating the red shift effects from the interband transition, has made the dimensional requirements of Al-based SRR more challenging than those based on other plasmonic metals. Other practical challenges include native surface oxidation of aluminum nanostructures, metal roughness, and most importantly cross-contamination during aluminum physical deposition step [34] that has been shown to suppress plasmonic oscillations. In this work, we attempt to address these challenges by fabricating aluminum SRR structures in the *u*-shape and the *v*-shape geometries, whose magnetic, electric, and magnetic-electric resonances all fall within the UV-Vis-NIR frequency spectrum. We discuss the mode excitations based on longitudinal and transverse plasmons, where the former corresponds to the well-known magnetic and electric modes in SRR, and the latter points to the unexplored hybrid magnetic-electric mode. In particular, we demonstrate that the preferential excitation of magnetic-electric mode over the fundamental magnetic mode becomes a limitation for the achievable magnetic resonances in aluminum SRR even before the fundamental kinetic inductance limitation sets in. Finally, we also discuss the interaction of these modes with aluminum interband transition, which results in the resonance splitting around 800 nm.

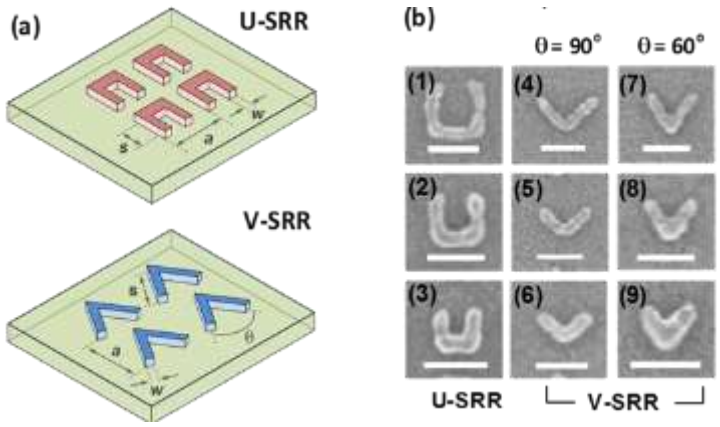

Figure 4. Aluminum split ring resonators (SRR) on ITO glass substrate. (a) Schematic representations of *u*-SRRs and *v*-SRRs with lattice constant *a*. (b) SEM images of the fabricated *u*-SRRs [1st column, (1)-(3)] and *v*-SRRs [2nd and 3rd column, (4)-(9)] with different resonator sizes (*s*) and opening angles (θ). The scale bar corresponds to 100 nm. The resonator sizes for the *u*-SRRs are 100 nm (1), 80 nm (2), and 60 nm (3); while for the *v*-SRRs are 100 nm (4, 7), 80 nm (5, 8), and 70 nm (6, 9). For all SRR structures, the lattice constant is designed to be two times the resonator size ($a = 2s$), and the feature width is 20-25 nm.

The *u*-SRR and *v*-SRR are schematically shown in Fig. 4a, with some of their smallest fabricated structures displayed in Fig. 4b. The experimentally measured transmissions of *u*-SRRs under *x* and *y* incidence polarizations are presented in Fig. 5a and 5b, respectively. We show the FDTD calculations of the *u*-SRR structures (indicated by the dashed lines), where we assume the presence of ~4-nm thick aluminum oxide layer

(Al_2O_3) on the SRR sidewalls. The fundamental and higher order magnetic modes are denoted by circles and triangles, respectively. As resonator size is decreased, it can be seen that the magnetic mode moves from ~1663 nm (s = 150 nm) to ~ 1271 nm (s = 70 nm), before interacting with the interband transition at s = 60 nm, giving split resonances at ~766 nm (m_{01} mode) and ~1042 nm (m_{02} mode). Meanwhile, at increasing resonator size, the higher order magnetic mode moves from ~452 nm (s = 60 nm) to ~530 nm (s = 70 nm) before interacting with the interband transition at s = 80 nm, resulting in split resonances at ~657 nm (m_{11} mode) and ~961 nm (m_{12} mode). The m_{11} mode then moves asymptotically around 800 nm at larger sizes, while m_{12} mode moves from ~961 nm (s = 80 nm) to ~1119 nm (s = 200 nm). The same observation is found under the y-polarization incidence (Fig. 5b), where the electric mode moves from ~558 nm (s = 60 nm) towards the interband transition, and results in resonance splitting at ~713 nm (e_{01} mode) and ~943 nm (e_{02} mode). The e_{01} mode then follows the same asymptotic path around 800 nm, while the e_{02} mode moves from ~943 nm (s = 80 nm) to ~1324 nm (s = 200 nm). As expected from the red shift from the aluminum interband transition, the achievable magnetic resonance frequencies remain lower than the gold and silver counterparts [13], [23], in spite of the higher free electron density in aluminum.

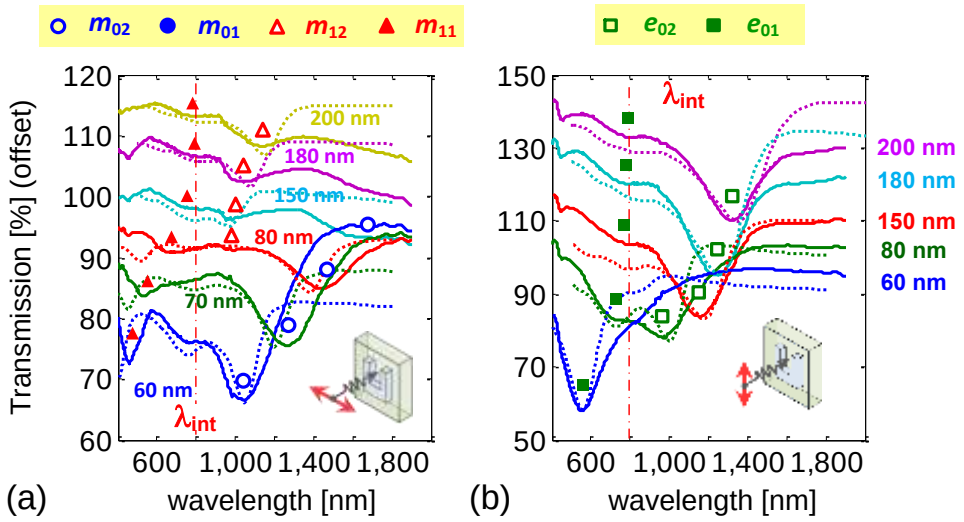

Figure 5. The resonance modes of aluminum u- SRR and their interactions with aluminum interband transition at λ_{int} = 800 nm. Near the interband transition, the fundamental magnetic mode (m_0) splits into m_{01} and m_{02} while the electric mode (e_0) splits into e_{01} and e_{02}. The experimental (solid) and calculated (dashed) transmission spectra of u-SRRs on ITO glass for (a) x-polarization, s = 60 – 100 nm, w = 25 nm, and (b) y-polarization, s = 120 – 200 nm, w = 40 nm. The fundamental magnetic modes are indicated by filled (m_{01}) and hollow (m_{02}) circles, while the higher order magnetic modes are indicated by filled (m_{11}) and hollow (m_{12}) triangles. The electric modes are indicated by filled (e_{01}) and hollow (e_{02}) squares.

As the SRR size from our previous works is constrained to s = 60 nm [13], [23], a different SRR geometry is clearly needed to further push the magnetic frequency into the short visible wavelength spectrum. This is accomplished by a *v*-shape SRR (Fig. 4b), which we believe can effectively reduce the SRR area (or SRR inductance) within the same dimensional constraints. In addition, the magnetic resonance can be more flexibly tuned in the *v*-SRR by virtue of its opening angle (θ) and size (s), as compared to that in the *u*-SRR which is tunable only by its resonator size (s). In another perspective, the tuning of resonance wavelength via the opening angle can also be understood as changing the SRR capacitance between SRR arms, which in turn leads to the tuning of SRR effective refractive index. [37] The experimental measurements are presented in Fig. 6, where the *v*-SRRs were fabricated by the same patterning process except for the 2-nm thick coating layer that was changed to titanium instead of nickel. This is because we found that titanium prevents native oxidation better than nickel. The experimental transmission spectra are shown in Fig. 6a and Fig. 6b for x and y polarizations, with their FDTD calculations denoted by dashed lines based on the same considerations as those in the *u*-SRR cases. The existence of m_{01} (squares) and m_{02} (circles) modes is again observed for θ = 90° and θ = 60° under the x polarization, where these modes are going into and out of interband transition at decreasing resonator sizes. For θ = 90°, the m_{01} moves from ~781 nm (s = 100 nm) to ~654 nm (s = 70 nm), while the m_{02} moves from ~1275 nm (s = 100 nm) to ~1035 nm (s = 80 nm). Likewise, for θ = 60°, the m_{01} moves from ~764 nm (s = 100 nm) to ~533 nm (s = 70 nm), while the m_{02} moves from ~1124 nm (s = 100 nm) to ~880 nm (s = 80 nm). Meanwhile, the me_0 mode (triangles) is observed around ~400 nm, which are more pronounced at decreasing resonator size for both opening angles. This lack of size dependence of me_0 positions supports the hypothesis that this is indeed the hybrid magnetic-electric mode (which is also verified numerically from our FDTD simulations). For θ = 90°, the me_0 positions are ~445 nm (for s = 80 nm) and ~410 nm (for s = 70 nm); while for θ = 60°, the me_0 positions are at ~437 nm (for s = 80 nm) and ~ 386 nm (for s = 70 nm), which already enters the ultraviolet regime.

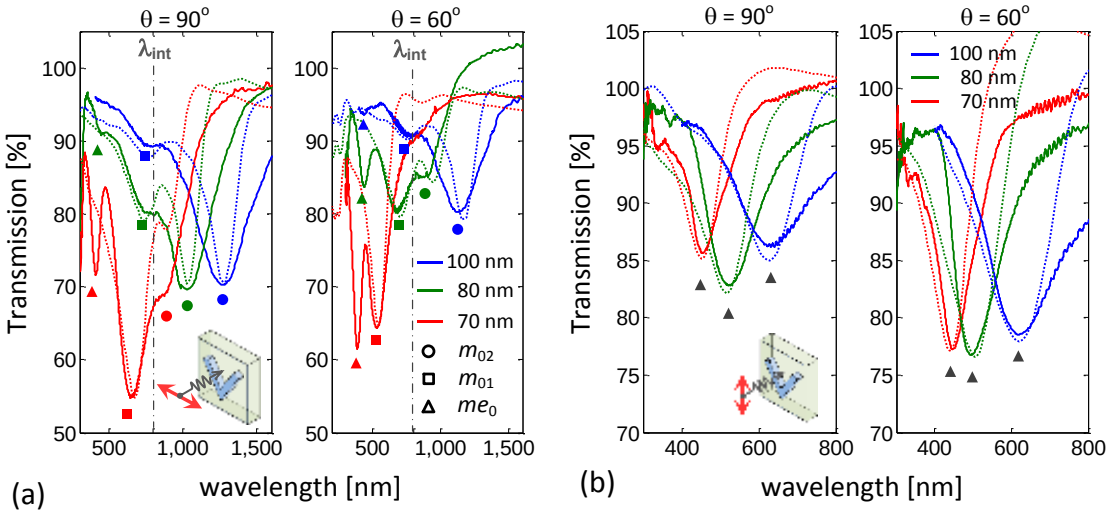

Figure 6. Mode excitation through longitudinal and transverse plasmons: (a) The *x*-polarized experimental (solid) and calculated (dashed) transmissions of *v*-SRRs of $\theta = 90^o$ and $\theta = 60^o$ for different sizes, where the split magnetic modes m_{01} (circles), m_{02} (squares), and the magnetic-electric mode me_0 (triangles) are all indicated; (b) The *y*-polarized experimental (solid) and calculated (dashed) transmissions of *v*-SRRs of $\theta = 90^o$ and $\theta = 60^o$ for different sizes, where the electric modes (e_0) are denoted by triangle markers.

For completeness, we also present the results of *v*-SRRs under the y polarization incidence (Fig. 6b), which show the traces of electric modes (denoted by triangle markers) at decreasing SRR size. For $\theta = 90^o$, the e_0 mode moves from ~630 nm (s = 100 nm) to ~454 nm (s = 70 nm), while for $\theta = 60^o$ the e_0 mode moves from ~619 nm (s = 100 nm) to ~446 nm (s = 70 nm). There are also subtle transmission dips around ~300 nm which likely originate from transverse plasmons along the *y*-direction. However, the resonance magnitude is independent of the resonator size, indicating that such a resonance dip comes from isolated transverse plasmons in the *y*-direction. This is in contrast to the me_0 mode which originates from the interaction between transverse plasmons in the *x*-direction. We further reduced the *v*-SRR size by decreasing the SRR opening angle to $\theta = 30^o$ (for s = 70 nm), with 14 nm lateral offset between the SRR arms to minimize e-beam proximity effects. From SEM inspection, the gap separation and the feature width are 28 nm and 21 nm, respectively, which we believe mark the smallest fabricated aluminum split ring resonator so far. Their measurements are presented in Fig. 7, where for clarity the inverse transmission spectra are plotted in log scale. For s = 80 nm, the resonance positions are ~604 nm (for m_{01} mode), ~481 nm (for e_{01} mode), and ~425 nm (for me_0 mode); while for s = 70 nm, ~469 nm (for m_{01} mode), ~ 429 nm (for e_{01} mode), and ~376 nm (for me_0 mode). It is interesting to note that m_{01} mode is progressively overshadowed by me_0 mode at decreasing SRR size, and that the m_{01} almost entirely diminishes in s = 70 nm. This clearly shows me_0 is more preferred to m_0 in the short visible wavelength, and we believe such a preferential excitation could serve as the other limitation for the achievable fundamental magnetic mode apart from the well-known kinetic inductance limitation [25], [26].

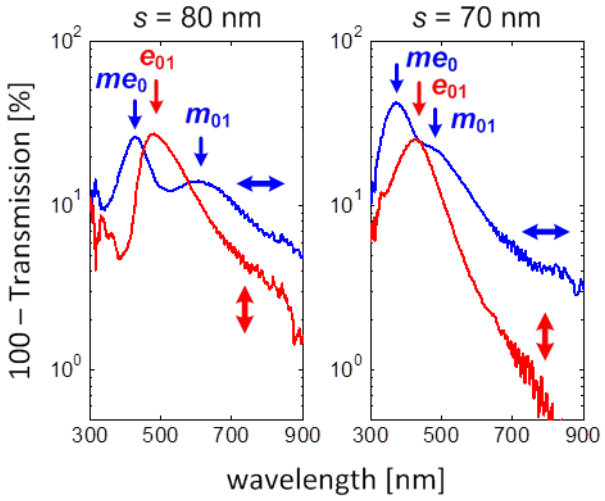

Figure 7. Preferential excitation of magnetic-electric mode in the ultraviolet spectrum. The magnetic, electric, and magnetic-electric modes of *v*-SRR (θ = 30° with 14 nm lateral offset between the arms) for *s* = 80 nm and *s* = 70 nm. The insets show the fabricated *v*-SRR, where the scale bars correspond to 100 nm. The gap separation and feature width are 28 nm and 21 nm, respectively.

(3) Rotationally symmetric gold nanostructures for robust and efficient biosensing applications [in preparation]

As a follow up of our previous work which showed that incorporating fourfold rotationally symmetric lattice could improve the optical response under unpolarized light illumination [13], various resonator designs with different rotational symmetry have been studied. We further explored different degrees of inherent rotational symmetry and studied their role in optical performances in the context of sensing application. From three-fold (C_3), four-fold (C_4), five-fold (C_5), six-fold (C_6), and eight-fold (C_8) rotational symmetry, we found that optical performance gets progressively better as the rotational symmetry is increased (see Fig. 8). We observe an enhancement in reflection (and scattering) by as much as ~1.6 times as the rotational symmetry is increased from $n = 3$ to $n = 8$ for a fixed arm length and period. In addition, we found that such resonant enhancement is caused by the interplay among longitudinal plasmons that are in conductive coupling with each other. The optical spectrum and resonance behavior of these structures have been theoretically studied and experimentally characterized, showing the figure-of-merit (FOM) of these structures in relation to sensing application.

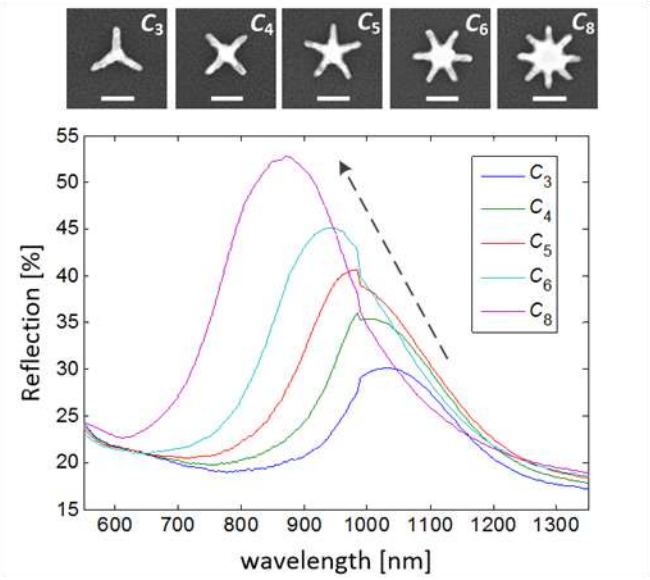

Figure. 8. The role of rotational symmetry in the resonance strength. The optical response increase progressively as the internal rotational symmetry changes from three-fold (n = 3) to n = 8 eight-fold (n = 8). The arm length (s) and periodicity (p) are s = 100 nm and p = 300 nm, respectively. The scale bars in all the insets represent 100 nm.

In terms of inter-resonator coupling, we have studied the evolution of resonance modes as the inter-resonator spacing is decreased. Of particular interest is the transition from isolated split ring resonator arrays in four-fold rotationally symmetric lattice (C_4 *u*-SRR) into a gammadion-type resonator with inherent fourfold rotational symmetry (U_f). Our numerical simulations show that as the inter-resonator gap decreases the magnetic mode (m_0) diminishes and the electric mode (e_0) split into two modes that eventually become hybrid magnetic-electric modes (me_0 and me_1). The first mode (me_0) is the longitudinal plasmons with magnetic characteristics, whose field distribution is qualitatively similar to that in m_0 mode for isolated SRR structure. On the other hand, the second mode (me_1) corresponds to higher order longitudinal plasmon. Experimentally (Figure 9), we observe that U_f structure exhibit much stronger scattering characteristics compared with isolated SRR (C_4 *u*-SRRs) of the same resonator size. The papers detailing these results are still in preparation.

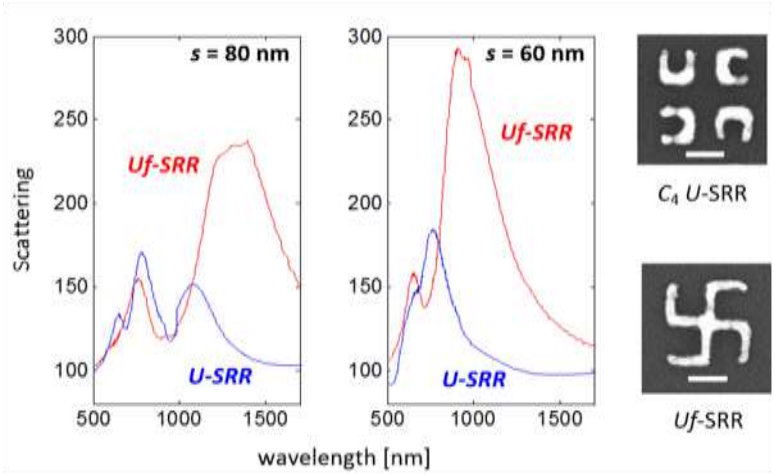

Figure 9. The effect of internal rotational symmetry in improving the optical response under unpolarized light illumination. The back scattering response of the Uf-SRR (red) and C_4 U-SRRs (blue) for s = 80 nm and s = 60 nm. Inset: the fabricated C_4 U-SRR and Uf-SRR. The scale bars represent 100 nm.

Acknowledgements
We thank AOARD for the financial support and Dr Hong Seng for his advice in conducting high quality research and great effort in coordinating and bridging collaboration with USA researchers..

References

[1] T. B. Hoang, G. M. Akselrod, and M. H. Mikkelsen, "Ultrafast Room-Temperature Single Photon Emission from Quantum Dots Coupled to Plasmonic Nanocavities."
[2] J. N. Farahani, D. W. Pohl, H. J. Eisler, and B. Hecht, "Single quantum dot coupled to a scanning optical antenna: A tunable superemitter," *Phys. Rev. Lett.*, vol. 95, no. 1, 2005.
[3] M. S. Eggleston, K. Messer, L. Zhang, E. Yablonovitch, and M. C. Wu, "Optical antenna enhanced spontaneous emission.," *Proc. Natl. Acad. Sci. U. S. A.*, vol. 112, no. 6, pp. 1704–9, 2015.
[4] R. F. Oulton, V. J. Sorger, T. Zentgraf, R.-M. Ma, C. Gladden, L. Dai, G. Bartal, and X. Zhang, "Plasmon lasers at deep subwavelength scale.," *Nature*, vol. 461, no. October, pp. 629–632, 2009.
[5] M. Peter, C. Friesen, and S. Linden, "Fabrication and characterization of active plasmonic antennas," no. September, pp. 10–12, 2015.
[6] L. Novotny and N. van Hulst, "Antennas for light," *Nat. Photonics*, vol. 5, no. 2, pp. 83–90, 2011.
[7] L. Novotny, "Optical Antennas: A New Technology that can Enhance Light-Matter Interactions," *Front. Eng.*, vol. 39, no. 4, pp. 100–120, 2012.
[8] S. Murugkar, I. De Leon, M. Horton, H. Qassim, J. Leach, and R. W. Boyd, "Planar chiral metamaterials for biosensing applications," *Spie ...*, vol. 8597, p. 85970Y, 2013.
[9] X. Xu, B. Peng, D. Li, J. Zhang, L. M. Wong, Q. Zhang, S. Wang, and Q. Xiong, "Flexible visible-infrared metamaterials and their applications in highly sensitive chemical and biological sensing," *Nano Lett.*, vol. 11, no. 8, pp. 3232–3238, 2011.
[10] W. Yue, Y. Yang, Z. Wang, L. Chen, and X. Wang, "Gold split-ring resonators (SRRs) as substrates for surface-enhanced raman scattering," *J. Phys. Chem. C*, vol. 117, no. 42, pp. 21908–21915, 2013.
[11] M. Svedendahl, S. Chen, A. Dmitriev, and M. Käll, "Refractometric Sensing Using Propagating versus Localized Surface Plasmons: A Direct Comparison," *Nano Lett.*, vol. 9, no. 12, pp. 4428–4433, Dec. 2009.
[12] B. Päivänranta, H. Merbold, R. Giannini, L. Büchi, S. Gorelick, C. David, J. F. Löffler, T. Feurer, and Y. Ekinci, "High aspect ratio plasmonic nanostructures for sensing applications," *ACS Nano*, vol. 5, no. 8, pp. 6374–6382, 2011.
[13] L. Y. M. Tobing, L. Tjahjana, D. H. Zhang, Q. Zhang, and Q. Xiong, "Deep subwavelength fourfold rotationally symmetric split-ring-resonator metamaterials for highly sensitive and robust biosensing platform.," *Sci. Rep.*, vol. 3, p. 2437, Jan. 2013.
[14] A. W. Clark, A. Glidle, D. R. S. Cumming, and J. M. Cooper, "Plasmonic split-ring resonators as dichroic nanophotonic DNA biosensors," *J. Am. Chem. Soc.*, vol. 131, no. 48, pp. 17615–17619, 2009.
[15] G. Sarau, B. Lahiri, P. Banzer, P. Gupta, A. Bhattacharya, F. Vollmer, and S.

Christiansen, “Enhanced Raman Scattering of Graphene using Arrays of Split Ring Resonators,” *Adv. Opt. Mater.*, vol. 1, no. 2, pp. 151–157, 2013.
[16] A. E. Cetin, D. Etezadi, and H. Altug, “Accessible Nearfields by Nanoantennas on Nanopedestals for Ultrasensitive Vibrational Spectroscopy,” *Adv. Opt. Mater.*, vol. 2, no. 9, pp. 866–872, 2014.
[17] A. Kosiorek, W. Kandulski, H. Glaczynska, and M. Giersig, “Fabrication of nanoscale rings, dots, and rods by combining shadow nanosphere lithography and annealed polystyrene nanosphere masks,” *Small*, vol. 1, no. 4, pp. 439–444, 2005.
[18] M. C. Gwinner, E. Koroknay, F. Liwei, P. Patoka, W. Kandulski, M. Giersig, and H. Giessen, “Periodic large-area metallic split-ring resonator metamaterial fabrication based on shadow nanosphere lithography,” *Small*, vol. 5, no. 3, pp. 400–406, 2009.
[19] A. I. Kuznetsov, A. E. Miroshnichenko, Y. H. Fu, V. Viswanathan, M. Rahmani, V. Valuckas, Z. Y. Pan, Y. Kivshar, D. S. Pickard, and B. Luk’yanchuk, “Split-ball resonator as a three-dimensional analogue of planar split-rings.,” *Nat. Commun.*, vol. 5, p. 3104, 2014.
[20] L. Y. M. Tobing, L. Tjahjana, and D. H. Zhang, “Direct patterning of high density sub-15 nm gold dot arrays using ultrahigh contrast electron beam lithography process on positive tone resist.,” *Nanotechnology*, vol. 24, no. 7, p. 75303, Feb. 2013.
[21] L. Y. M. Tobing, L. Tjahjana, and D. H. Zhang, “Large contrast enhancement by sonication assisted cold development process for low dose and ultrahigh resolution patterning on ZEP520A positive tone resist,” *J. Vac. Sci. Technol. B Microelectron. Nanom. Struct.*, vol. 30, no. 5, p. 51601, 2012.
[22] L. Y. M. Tobing, L. Tjahjana, and D. H. Zhang, “Sub-10-nm size and sub-40-nm pitch metal dot patterning for low-cost bit patterned media application,” *Nanotechnology, IEEE Trans.*, vol. 13, no. 3, pp. 496–501, May 2014.
[23] L. Y. M. Tobing, L. Tjahjana, D. H. Zhang, Q. Zhang, and Q. Xiong, “Sub-100-nm Sized Silver Split Ring Resonator Metamaterials with Fundamental Magnetic Resonance in the Middle Visible Spectrum,” *Adv. Opt. Mater.*, vol. 2, no. 3, pp. 280–285, Mar. 2014.
[24] L. Y. M. Tobing, Y. Luo, K. S. Low, D. Zhang, and D. H. Zhang, “Observation of the Kinetic Inductance Limitation for the Fundamental Magnetic Resonance in Ultrasmall Gold v -Shape Split Ring Resonators,” *Adv. Opt. Mater.*, vol. 4, no. 7, pp. 1047–1052, Jul. 2016.
[25] M. W. Klein, C. Enkrich, M. Wegener, C. M. Soukoulis, and S. Linden, “Single-slit split-ring resonators at optical frequencies: limits of size scaling.,” *Opt. Lett.*, vol. 31, no. 9, pp. 1259–1261, 2006.
[26] J. Zhou, T. Koschny, M. Kafesaki, E. N. Economou, J. B. Pendry, and C. M. Soukoulis, “Saturation of the magnetic response of split-ring resonators at optical frequencies,” *Phys. Rev. Lett.*, vol. 95, no. 22, 2005.
[27] L. Y. M. Tobing and D.-H. H. Zhang, “Preferential Excitation of the Hybrid Magnetic--Electric Mode as a Limiting Mechanism for Achievable Fundamental Magnetic Resonance in Planar Aluminum Nanostructures,” *Adv. Mater.*, vol. 28, no. 5, pp. 889–896, Feb. 2015.
[28] P. B. Johnson and R. W. Christy, “Optical constants of the noble metals,” *Phys. Rev. B*, vol. 6, no. 12, pp. 4370–4379, 1972.
[29] P. R. West, S. Ishii, G. V. Naik, N. K. Emani, V. M. Shalaev, and A. Boltasseva, “Searching for better plasmonic materials,” *Laser and Photonics Reviews*, vol. 4, no. 6.

pp. 795–808, 2010.
[30] P. Tassin, T. Koschny, M. Kafesaki, and C. M. Soukoulis, “A comparison of graphene, superconductors and metals as conductors for metamaterials and plasmonics,” *Nat. Photonics*, vol. 6, no. 4, pp. 259–264, 2012.
[31] M. W. Knight, L. Liu, Y. Wang, L. Brown, S. Mukherjee, N. S. King, H. O. Everitt, P. Nordlander, and N. J. Halas, “Aluminum plasmonic nanoantennas,” *Nano Lett.*, vol. 12, no. 11, pp. 6000–6004, 2012.
[32] Y. Ekinci, H. H. Solak, and J. F. Löffler, “Plasmon resonances of aluminum nanoparticles and nanorods,” *J. Appl. Phys.*, vol. 104, no. 8, 2008.
[33] I. Zorić, M. Zäch, B. Kasemo, and C. Langhammer, “Gold, platinum, and aluminum nanodisk plasmons: Material independence, subradiance, and damping mechanisms,” *ACS Nano*, vol. 5, no. 4, pp. 2535–2546, 2011.
[34] M. W. Knight, N. S. King, L. Liu, H. O. Everitt, P. Nordlander, and N. J. Halas, “Aluminum for plasmonics,” *ACS Nano*, vol. 8, no. 1, pp. 834–840, 2014.
[35] B. Lahiri, S. G. Mcmeekin, A. Z. Khokhar, R. M. De La Rue, and N. P. Johnson, “Magnetic response of split ring resonators (SRRs) at visible frequencies.,” *Opt. Express*, vol. 18, no. 3, pp. 3210–8, 2010.
[36] S. Linden, C. Enkrich, G. Dolling, M. W. Klein, J. Zhou, T. Koschny, C. M. Soukoulis, S. Burger, F. Schmidt, and M. Wegener, “Photonic metamaterials: Magnetism at optical frequencies,” *IEEE J. Sel. Top. Quantum Electron.*, vol. 12, no. 6, pp. 1097–1104, 2006.
[37] K. Kishor, M. N. Baitha, R. K. Sinha, and B. Lahiri, “Tunable negative refractive index metamaterial from V-shaped SRR structure: fabrication and characterization,” *J. Opt. Soc. Am. B*, vol. 31, no. 7, p. 1410, 2014.

3. List of publications and significant collaborations that resulted from your AOARD supported project:

(a) Papers published in peer-reviewed journals (all papers acknowledged AOARD’s support)

[1] L. Y. M. Tobing, G. Y. Goh, A. D. Mueller, L. Ke, and D. H. Zhang, “Rotationally symmetric plasmonic nanostructures for sensing applications,” (in preparation)
[2] L. Y. M. Tobing, Y. Luo, K. S. Low, D. Zhang, and D. H. Zhang, “Observation of the Kinetic Inductance Limitation for the Fundamental Magnetic Resonance in Ultrasmall Gold v -Shape Split Ring Resonators,” *Adv. Opt. Mater.*, vol. 4, no. 7, pp. 1047–1052, Jul. 2016.
[3] L. Y. M. Tobing and D.-H. H. Zhang, “Preferential Excitation of the Hybrid Magnetic--Electric Mode as a Limiting Mechanism for Achievable Fundamental Magnetic Resonance in Planar Aluminum Nanostructures,” *Adv. Mater.*, vol. 28, no. 5, pp. 889–896, Feb. 2015.
[4] S. Qiu, L. Y. M. Tobing, J. Tong, Y. Xie, Z. Xu, P. Ni, and D.-H. Zhang, “Two-dimensional metallic square-hole array for enhancement of mid-wavelength infrared photodetection,” *Opt. Quantum Electron.*, vol. 48, no. 3, p. 203, Mar. 2016.
[5] J. Tong, Y. Xie, Z. Xu, S. Qiu, P. Ni, L. Y. M. Tobing, and D.-H. Zhang, “Study of dual color infrared photodetection from n-GaSb/n-InAsSb heterostructures,” *AIP Adv.*, vol. 6, no. 2, p. 25120, 2016.

[6] Z. Xu, L. Y. M. Tobing, Y. Xie, J. Tong, P. Ni, S. Qiu, T. Yu, and D. H. Zhang, "Aluminum based structures for manipulating short visible wavelength in-plane surface plasmon polariton propagation," *Opt. Express*, vol. 23, no. 17, p. 22883, Aug. 2015.

(b) Papers published in peer-reviewed conference proceedings(all papers acknowledged AOARD's support)

[1] L. Y. M. A. Tobing, D. Zhang, K. S. Low, and D. H. Zhang, "Gold and silver resonators and their optical properties," *Int. J. Nanotechnol.*, vol. 13, no. 7, p. 561, 2016.
[2] Z. Xu, L. Y. M. Tobing, D. Zhang, and D. H. Zhang, "Cogwheels for generation of surface plasmon polariton vortex," *Int. J. Nanotechnol.*, vol. 12, no. 10/11/12, p. 909, 2015.
[3] S. Qiu, L. Y. M. Tobing, Z. Xu, J. Tong, P. Ni, and D.-H. Zhang, "Surface Plasmon Enhancement on Infrared Photodetection," *Procedia Eng.*, vol. 140, pp. 152–158, 2016.
[4] J. Tong, Y. Xie, P. Ni, Z. Xu, S. Qiu, L. Y. M. Tobing, and D.-H. Zhang, "InAs 0.91 Sb 0.09 photoconductor for near and middle infrared photodetection," *Phys. Scr.*, vol. 91, no. 11, p. 115801, Nov. 2016.

(c) Papers published in non-peer-reviewed journals and conference proceedings

None

(d) Conference presentations without papers

None

4. Keynote and Invited talks

[1] L. Y. M. TOBING and Dao Hua ZHANG, (Invited talk) "Split ring resonators from Infrared to UV range", Collaborative conference on 3D and Materials Research (CC3DMR), 20-24 June, 2016, Incheon/Seoul, South Korea.
[2] Yunjiang Jin, Peinan Ni, Xaiohong Tang and Dao Hua Zhang*, "Antimony-based III-V materials for infrared photodetection", 19th International Conference on Superlattices, Nanostructures and Nanodevices (ICSNN 2016) that will be held in Hong Kong, 25-30 July 2016. (International advisory committee)
[3] D. H. Zhang, (Keynote) "Semiconducting materials for photonic technology", April 17-19, 2016 Suzhou, China
[4] D. H. Zhang (Keynote), "Subwavelength metallic structures and applications", The 2nd International Conference on Advance Materials Research and Application (AMRA 2015), Dec 18-21, 2015

[5] L.Y.M.A. Tobing and Dao-Hua Zhang, (Invited talk), "Split-Ring Resonators for Optical Frequencies", International conference on Nanophonics, 25-28 May 2015, Changchun, China

5. Award of fund received related to your research efforts (name, amount, date):

Project name/Title	**Amount ($)**	**Date**
Broadband Plasmonic Devices for Biosensing and Optoelectronic Modulation (MOE- M4020283.040)	935,080	11-2015
Transformation Optics for Low-loss Plasmonic Circuitry	200,000	11-2015
CMOS Surface Plasmon Polariton Interconnect for Tera-scale On-chip Communication (RG 74/15)	160,000	11-2015
3D split ring resonator arrays in UV-visible range for biochemical sensing	918,090	Submitted
Surface plasmon enhanced high operating temperature two-dimensional focal plane array midwave infrared cameras.	1,185,000	Submitted